



OPEN

A mechanical insight into the triggering mechanism of frequently occurred landslides along the contact between loess and red clay

Baoqin Lian¹, Xingang Wang¹✉, Kai Liu¹, Sheng Hu² & Xiao Feng³

The triggering mechanism and movement evolution of loess-red clay landslides, which occurred frequently along the contact between the loess and red clay on the Loess Plateau, are closely related to the mechanical properties of the contact surface. This work presents an experimental investigation on loess, clay and loess-red clay interlaminar (LRCI) samples obtained from a typical loess-red clay landslide in northern part of Shaanxi province of China, using a series of ring shear tests, microscopic observation and scanning electron microscopy tests, in an attempt to explore the mechanical behavior of loess, clay and LRCI samples with variation in moisture content, normal stress and shear rate. The results revealed that for all specimens, both the peak shear strength τ_p and the residual shear strength τ_r decreased with increasing moisture content, among which, moisture content has the greatest influence on the τ_p and τ_r of red clay, followed by the LRCI specimen, and the loess specimen is least affected by moisture content. Meanwhile, exponential functions describing the correlations between shear strength and moisture content of LRCI, red clay and loess specimens were proposed. Furthermore, the macroscopic morphological characteristics and the microstructure of shear surface obtained from the LRCI specimens showed that a localized water accumulation was built up within the shear surface as the water content increases to some extent, and a high degree of liquefaction developed within shear surface when the moisture content reached to the saturate degree. The microstructural observation on LRCI specimen suggested that the shear surface became smoother and the larger percentage of small-sized pores was observed with moisture content. Accordingly, the built-up excess pore water pressure during shearing is difficult to be dissipated due to a close structure of small-sized pores. Due to the low permeability, high pore-water pressure built up within the shear zone and the increase in the fine particle content, the LRCI soils with a high saturation degree shows the potential for the localized liquefaction within shear zone, which further provides a scientific explanation for the triggering mechanism of loess-red clay landslides with high-speed and long-run out.

Loess landslides have been recognized as one of the most common geologic hazards on the Loess Plateau of China^{1,2}. According to the composition of the slide mass and the situation of the failure plane, four types of landslide have been identified: 'slides within loess', 'bedrock contact landslides', 'palaeosol contact landslides' and 'mixed landslides'³⁻⁵. Among four types of loess landslides, landslides occur along the contact between loess soils and red clay make up the most percentage of landslides throughout the Chinese Loess Plateau³. Some catastrophic loess landslides occurring along the contact between loess soils and red clay had been reported in China, causing severe casualty almost every year^{6,7}.

Catastrophic loess landslides can occur in various soil types, such as loess soils, residual soils and sensitive clays. It is generally understood that these loess landslides are related to the decrease in the shear strength of slip

¹State Key Laboratory of Continental Dynamics, Department of Geology, Northwest University, Xi'an 710069, China. ²College of Urban and Environmental Science, Northwest University, Xi'an 710127, China. ³State Key Laboratory of Petroleum Resources and Prospecting, China University of Petroleum (Beijing), Beijing 102249, China. ✉email: xgwang@nwu.edu.cn

zone soils. It has been found that the characteristics of slip zone soils plays a key role in the evolution of a loess landslide^{8–10}. The contact interface between loess soils and red clay easily develops into a weak surface, which would eventually evolve into a sliding surface^{11,12}, affecting the occurrence of landslides^{3,13}. For example, it was reported that the average area and length of red clay contact landslides are 5.52 and 2.45 times larger than those of landslides occurred within loess¹⁴, and numerous researchers have pointed out that the mechanical characteristics of a contact surface between loess soils and red clay^{2,6,15} is a basic factor controlling the occurrence frequency and extent of a Loess-Red clay landslide on the Loess Plateau^{10,16,17}. Therefore, understanding the mechanical properties of slip zone soils is of great significance to get deeper insight into the triggering mechanism of a loess-red clay landslide^{12,18}.

To date, there has been considerable research into understanding the mechanical properties of slip zone soils with main efforts on examining the shear behavior of slip zone soils collected from loess landslides^{19–21}. There have also many attempts to investigate the shear behavior of slip zone soils^{11,22}, with main focus on the landslides occurred along the paleosol contact surface. These researches enabled us to understand the basic mechanical behavior of slip zone soils, and some factors influencing the evolution and movement of landslides. However, compared to those slip zone soils obtained from loess landslides and paleosol contact landslides, the studies on the mechanical characteristics of slip zone soils of loess-red clay landslides are rare, but have been reported by some researchers¹³. In previous studies, Wen, Wang²³ explored the deformation process of a loess-red clay landslide by using the field monitoring and laboratory physical modeling and found that rainfall has a significant impact on the deformation characteristics of slopes through its interaction contact between the loess soil and the loess-Neogene red mudstone, while the variation in the residual strength of slip zone soils during the shearing process was not mentioned. Using the pipette method and fine X-ray diffraction method, Shi et al.⁷ pointed out that rainfall gradually destroyed the structure of the Neogene clay and transformed it into slip zone soils, which causes the shear strength of the Neogene clay to decrease and the ground water table level to rise as well. However, the mechanical properties of slip zone soils was not investigated. Furthermore, Zhang et al.¹⁰ investigated the shear surface behavior of red clay samples obtained from loess-red clay landslides through a series of dynamic triaxial tests and reported that the shear strength of clay degenerated more in the cyclic triaxial tests compared to that in the static triaxial tests, while microstructure characteristics of soils was not mentioned, and the advanced apparatus which could better determine the strength parameters of slip zone soils was not been used^{24,25}. The review of the literature enabled us to know that the mechanical characteristics of slip zone soils as well as the factors affecting the occurrences of loess-red clay landslides still requires experimental evidence.

To better examine triggering mechanism of landslides occurred along the contact between loess and red clay, Loess-red clay interlaminar (LRCI) samples were used to conduct a series of ring shear tests in this study. In addition, ring shear tests results using loess samples and red clay samples were compared with that using LRCI samples. Furthermore, the effect of moisture content (Mc), normal stress (σ_n) and shear rate (v) on the shear strength was concluded and the relationships between shear strength and moisture content were obtained for LRCI, red clay and loess specimen. Finally, the influence of moisture content on the macroscopic morphology, microstructure characteristics and quantitative micro-pore parameters of the shear surface of LRCI specimen were discussed as well. The result is apt to provide experimental and theoretical basis for interpreting the triggering mechanism of such kind landslides, predicting the landslide evolution, and handling loess-red clay landslide problems.

Materials and Methods

Testing sample. Disturbed soil samples used in this study were taken from a landslide (36.84°N, 108.61°E) that occurred at an elementary school in Zhidan County, Shaanxi, China, which is located in the hinterland of the Loess Plateau (Fig. 1a). The landslide is recognized as a catastrophic landslides due to its high speed and long run-out distance²⁶. The upper part of the sliding mass is covered with a thick layer of loess that is characterized by lots of pores and well-developed cracks (see the red arrow in Fig. 1b). The main direction of the landslide is 168° north to east (Fig. 1c). In the lower part of the sliding mass, a dense structure of Pliocene red clay was found, with a thickness of about 3 m to 6 m (Fig. 1d). The sliding mass with the average slope 41° has a relative height difference of 103 m (Fig. 1e), the length of 174 m and the width of 172 m, covering area approximately 24,080 m². The red clay has been identified as slip zone soil as the sliding scratches are obviously visible on the surface of the red clay at the slip zone (Fig. 2). Table 1 lists the physical parameters of loess and red clay which were collected for testing. As for red clay samples, clay content accounts for about 56.4% and main mineral components such as montmorillonite and illite are dominated. The red clay appears dark red as it contains relatively more proportions of free iron oxide, indicating that the red clay is formed in semi-arid and humid climate environment. The collected loess and red clay samples were completely air-dried, crushed and sieved through a 2 mm mesh screen, and then kept in an oven at 105 °C for more than 24 h to fully dry for sample preparation.

Testing apparatus. Extensive literatures have documented that the residual shear strength (τ_r) of slip zone soil is an important parameter for analysis and assessing the stability of slopes^{27–29}. Methods currently used to measure the residual shear strength mainly include triaxial compression tests, reversal direct shear tests^{30,31} and ring shear tests^{32–34}. By now, it has also been found that the use of the triaxial compression tests to determine residual shear strength of soil is not a first choice³⁵. Compared with triaxial compression tests and direct shear test, ring shear tests enable simulating characteristics of slip zone soil in field with a large shearing displacement and keeping the shearing direction of specimen unchanged^{36,37}.

Ring shear apparatus (SRS-150) manufactured by GCTS company of the United States was adopted in this research (Fig. 3a). In experimental process, the specimen is consolidated under a specific value of normal stress until the required consolidation was achieved. Then, the consolidated specimen is subjected to shearing by

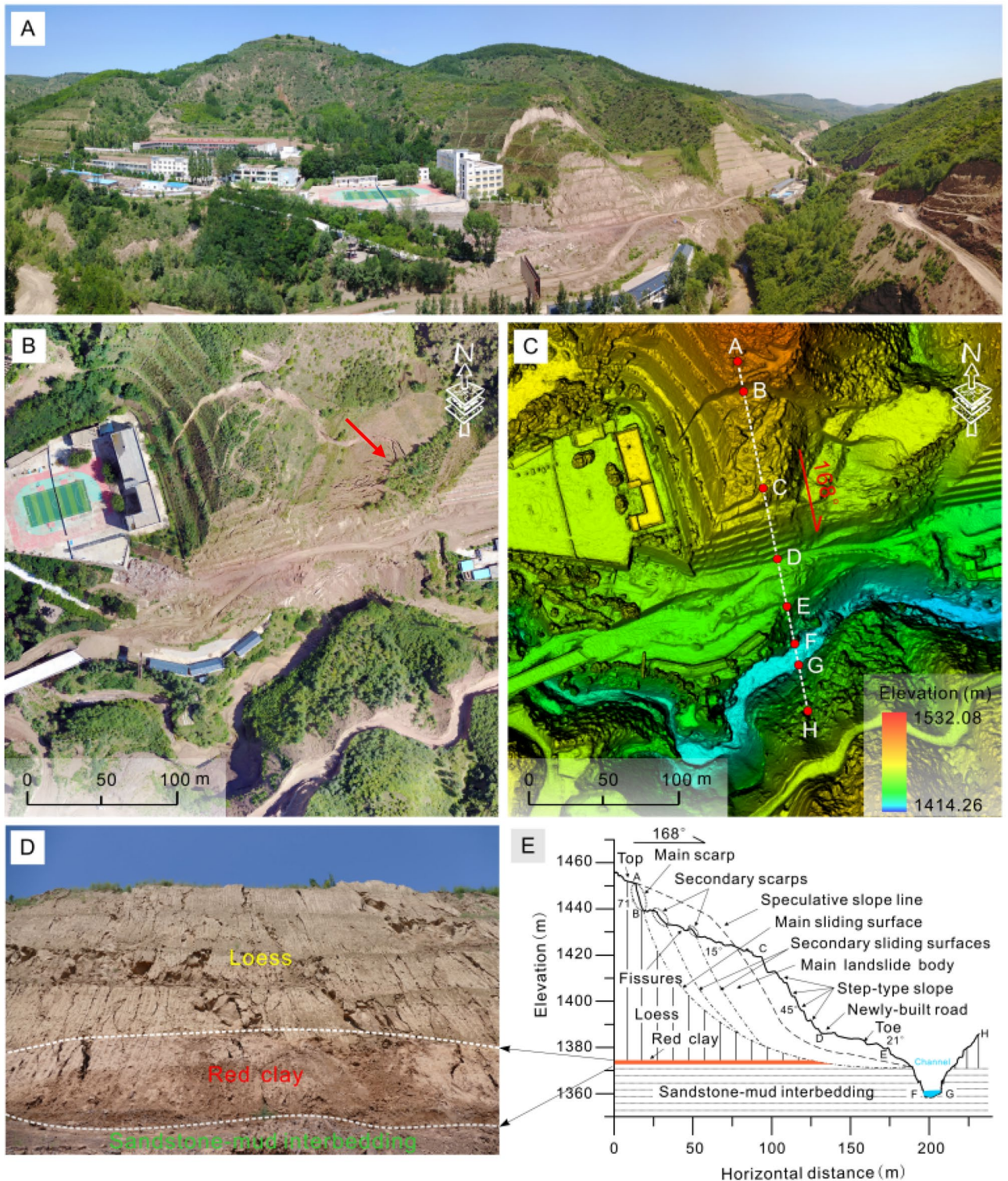


Figure 1. Loess-red clay landslide in Zhifang village elementary school. (a) Overview of landslide; (b) landslide crack; (c) DEM image of landslide; (d) landslide stratum; (e) sectional view of the main sliding direction of the landslide.

rotating the lower half of the shear box to obtain the shear strength and deformation of the specimen, while the upper half is fixed. The shear box has the inner diameter of 100 mm, the outer diameter of 150 mm (Fig. 3b), and the sample height of 25 mm. The ring shear rate can be controlled in the range of 0.001°/min to 360°/min. In this study, the shear plane on its upper half of the platen was used to analyze (Fig. 3c).



Figure 2. Sliding scratch surfaces and sampling site. (a) The landslide boundary; (b) sampling site; (c) sliding scratch surfaces.

Material	ρ	ρ_d	W_n	W_s	W_L	W_p
Loess	1.76	1.48	16	28	32	21
Red clay	2.08	1.81	19.26	26	38.95	21.2

Table 1. Physical parameters of Lishi loess used in the test. ρ = Natural density (g/cm^3); ρ_d = Dry density (g/cm^3); W_n = Natural water content (%); W_s = saturated moisture (%); W_L = Liquid limit (%); W_p = Plastic limit (%).

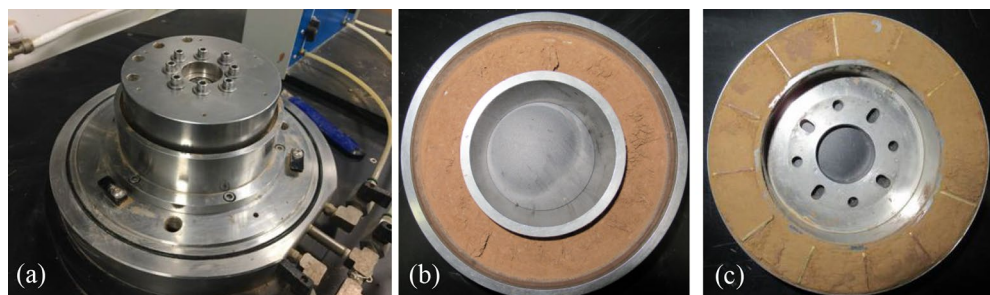


Figure 3. A sheared specimen. (a) Ring shear chamber; (b) the bottom platen with sheared soil; (c) the top platen with sheared soil.

Testing procedure. As mentioned above, the variation in the moisture content, normal stress and shear rate would result in the change in the mechanical properties of soils. To examine the effect of the variation of moisture content, normal stress and shear rate on the shear characteristics of soils, nine groups of three remolded specimens each have been prepared for the shear tests (Table 2). For each kind of soils (loess, red clay and LRCI), one group was tested at the normal stress of 200 kPa, shear rate of 1 mm/min ($w = 12\%$, 20% and 28%), while the other two groups were tested at the moisture content of 12% and shear rate of 1 mm/min ($\sigma_n = 100, 200$ and 300 kPa),

w(%)	σ_n (kPa)	v(mm/min)
12	200	1
20		
28		
12	100	1
	200	
	300	
12	200	0.01
		0.1
		1

Table 2. Ring shear test scheme.



Figure 4. Shear planes of specimen after ring shear tests. (a) Loess; (b) red clay; (c) LRCI.

at the moisture content of 12% and normal stress of 200 kPa ($v = 0.01, 0.1$ and 1 mm/min), respectively. According to the physical parameters of soils listed in Table 1, the maximum and natural water content of Lishi loess are approximately 28.0% and 16% respectively, which means the water content of soils in the field varies widely and may exert considerable control on the mechanical properties of soils. Samples with moisture contents of 12% (less than 16%), 20% and 28% (equals to saturated water content) were prepared in this study.

The sample for each test was prepared by the following procedures: the samples were packed in plastic bags and kept in a sealed container for about 48 h to allow water fully migrated within the specimen. To study the mechanical properties of LRCI sample, it is necessary to prepare an artificial shear plane of the loess-clay interlaminar. In this study, an artificial shear plane of loess-clay interlaminar was prepared by following procedures: Firstly, the red clay is placed in the shear box and consolidated using a specific normal stress according to the testing scheme (Table 2). The consolidated specimen was sheared until soil sample forms a continuous annular shear plane. Secondly, the upper shear box was removed and the red clay in the lower shear box was retained (see Fig. 3b). And then the red clay in the upper shear box was cleaned, the same thickness of loess was deposited into the upper shear box to ensure that the shear plane is located at the junction of red clay and loess while re-shearing. Finally, the upper shear box was installed again, and the loess-red clay specimen was consolidated under the original normal stress level. Thus, LRCI specimen with the fixed shear plane is prepared. During ring shear tests, loess samples and red clay samples are weighed separately and then placed into the shear chamber, and then the axial load is applied to the samples to achieve a required consolidation. Subsequently, the consolidated specimen is sheared until the residual state (i.e., the shear resistance value was kept at a constant value without further changing with progress of shearing) is achieved. Figures 4a–c show shear planes of three kinds of specimen after ring shear tests.

Verification of test stability. To test the stability of the device, two groups of comparison tests were performed, using saturated loess soils and saturated red clay at the normal stress of 200 kPa, shear rate of 1 mm/min. The results are shown in Fig. 5. Figure 5a compares the results of remolded specimens of saturated loess soils, while Fig. 5b depicts the results of remolded specimens of saturated red clay. As can be seen in Fig. 5a,b, for the saturated loess soils and red clay, the stress-displacement curves of two sets of comparative tests are almost identical, indicating that the data obtained using the device is accurate and repeated tests with a good stability and high precision can be ensured by using this device.

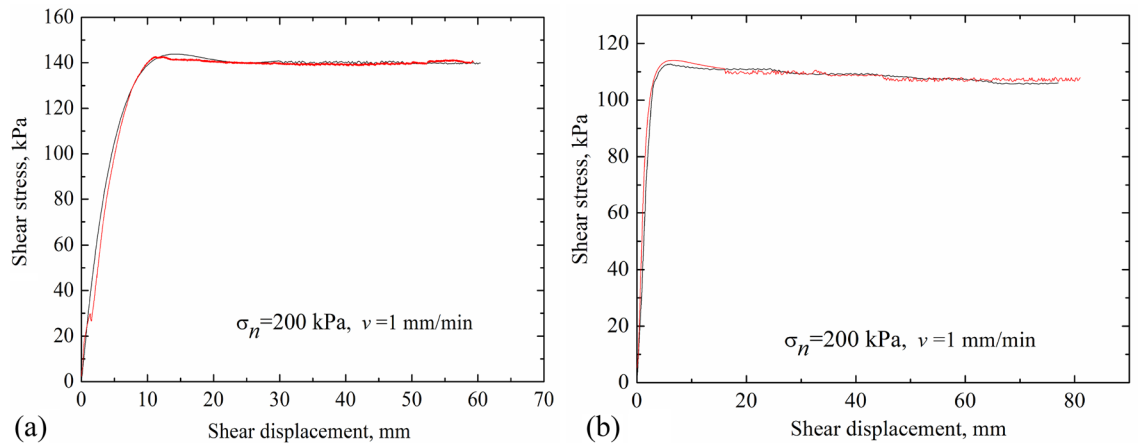


Figure 5. Verification of stability of the ring shear test. (a) Saturated loess; (b) saturated red clay.

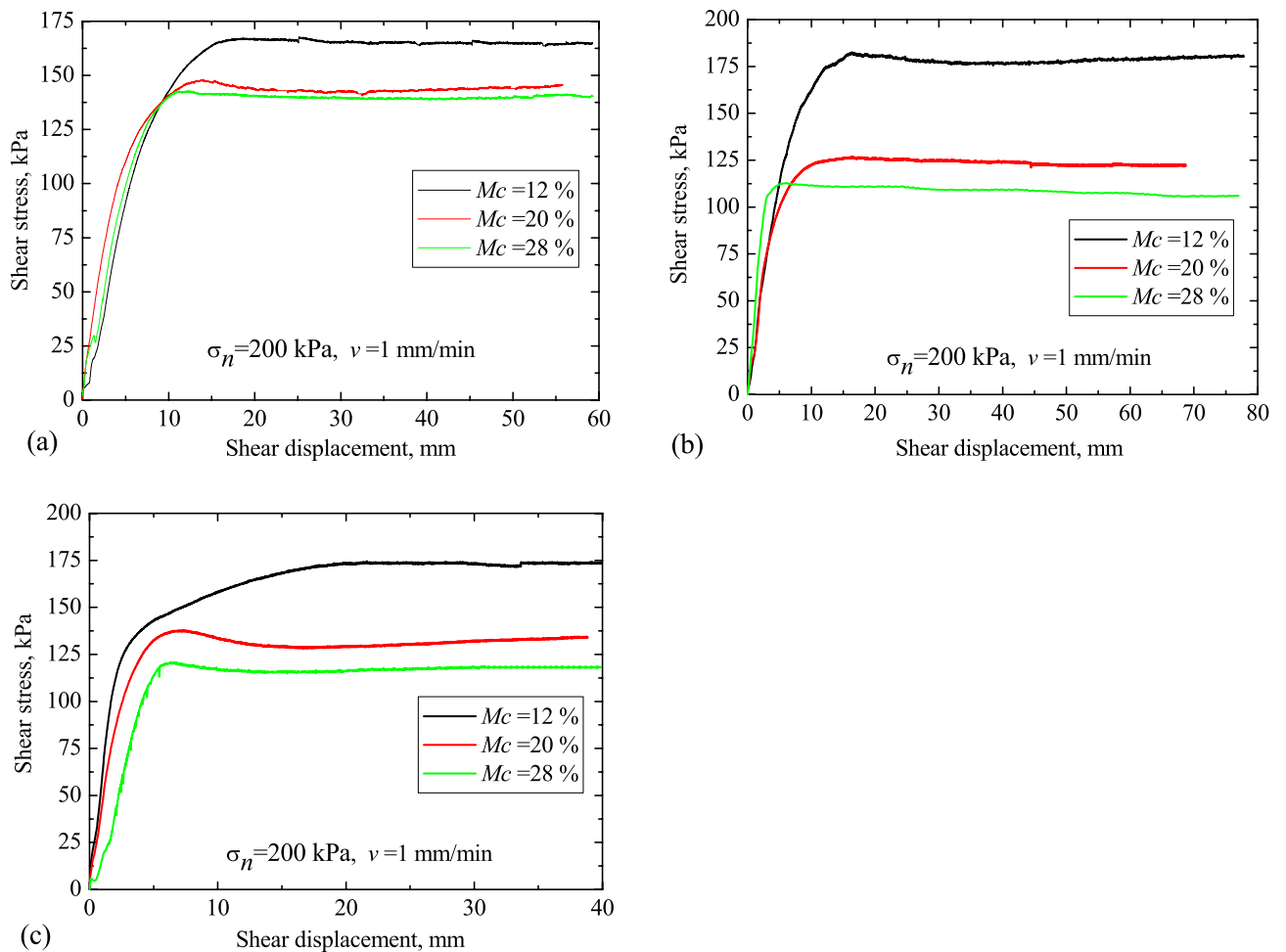


Figure 6. Stress–displacement curves under different moisture contents. (a) Loess; (b) red clay; (c) LRCI.

Results

The typical shear stresses for loess, red clay and LRCI specimen are plotted in Figs. 6, 7 and 8, respectively, against the shear displacement. In addition, according to the stress-displacement curves, histograms depicting the peak strength (denoted as τ_p) and residual strength (denoted as τ_r) of soils are shown in Fig. 9. In current study, residual strength was determined following Salih et al.³⁸ who suggested that the residual strength is attained if a relatively constant shear stress is measured for more than half hour. However, a constant value of residual strength was not observed due to the stress fluctuation in the shearing process, even the specimen was sheared

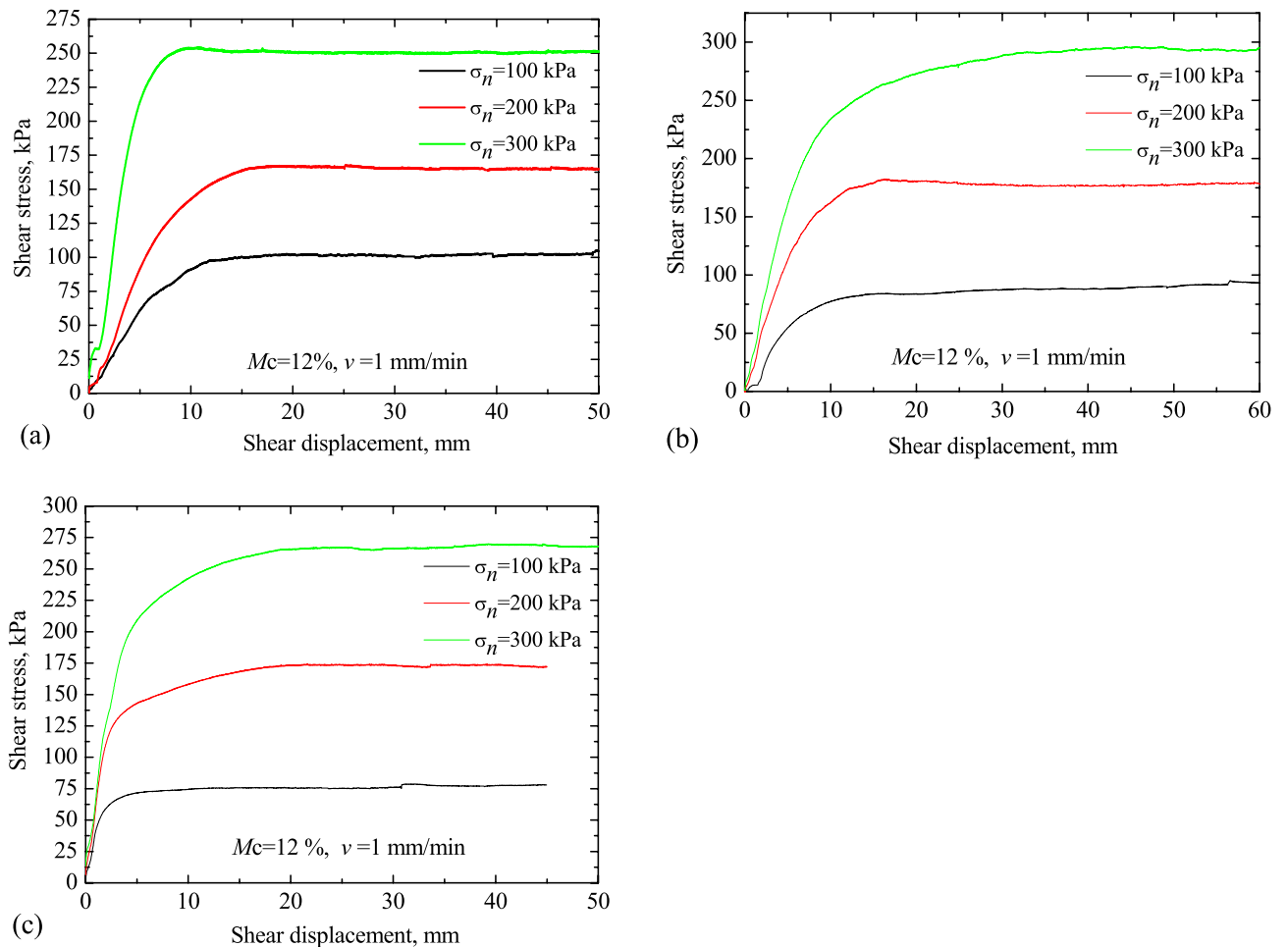


Figure 7. Stress–displacement curves under different normal stress. (a) Loess; (b) red clay; (c) LRCI.

at a large displacements. Thus, over a certain period (more than half hour), the lowest shear resistance that was kept at a roughly stable value was adopted as the residual strength in this study.

Shear behavior. Moisture content has been recognized as a fundamental factor affecting shear properties of soil^{21,39,40}. The experimental results of three samples with moisture contents of 12%, 20% and 28%, are selected to illustrate the effect of the moisture content on the shear behavior of soil samples. When $\sigma_n = 200$ kPa and $v = 1$ mm/min, the typical shear behavior of specimens is shown in Fig. 6, where the shear stress is plotted against the shear displacement. As shown in Fig. 6, the response curves are almost similar for all samples for testing. However, in comparison to the loess and red clay (Fig. 6a,b), the shear resistance of LRCI reaches its peak after a larger displacement (more than 10%), and then shows a small decrease with further shearing (Fig. 6c). Meanwhile, it can be noted that for a specific specimen, the peak shear strength as well as the residual shear strength decreases with increasing moisture content (Fig. 9a,b)). Moreover, among three kinds of specimen, the moisture content has the greatest influence on the τ_p and τ_r of red clay, followed by LRCI specimen and the loess specimen is least affected by moisture content. To be more specific, an increase in M_c (from 12 to 28%) of red clay causes a considerable reduction in τ_r (from 180.02 kPa to 105.76 kPa). Comparatively, for LRCI specimen, τ_r tends to decrease from 173.42 kPa to 117.68 kPa when M_c increases from 12 to 28%, decreasing about 32%. And for loess specimen, τ_r decreased from 165.28 kPa to 140.66 kPa with M_c increased from 12 to 28%, decreasing approximately 15% (Fig. 9b).

However, it is seen that, for a given moisture content, the comparison in τ_r among three kinds of specimen is complicated (Fig. 9b). For example, at M_c of 12%, τ_r of red clay (180.02 kPa) is greater than that of LRCI (173.42 kPa), and τ_r of loess (165.28 kPa) is the minimum. Nevertheless, τ_r of loess (145.49 kPa) is slightly higher than that of LRCI (133.89 kPa) with M_c of 20%, and the minimum τ_r of red clay is obtained at M_c of 20%, reaching about 122.12 kPa. In addition, the τ_r of loess, LRCI and red clay is 140.66 kPa, 117.68 kPa and 105.76 kPa, respectively, when M_c is 28%. The experimental results herein suggested that when moisture content is above a certain value, the shear strength of the red clay and LRCI will be greatly less than that of loess soils.

Based on the experimental data (Fig. 9a, b), the relationships between shear strength and moisture content are shown in Fig. 10.

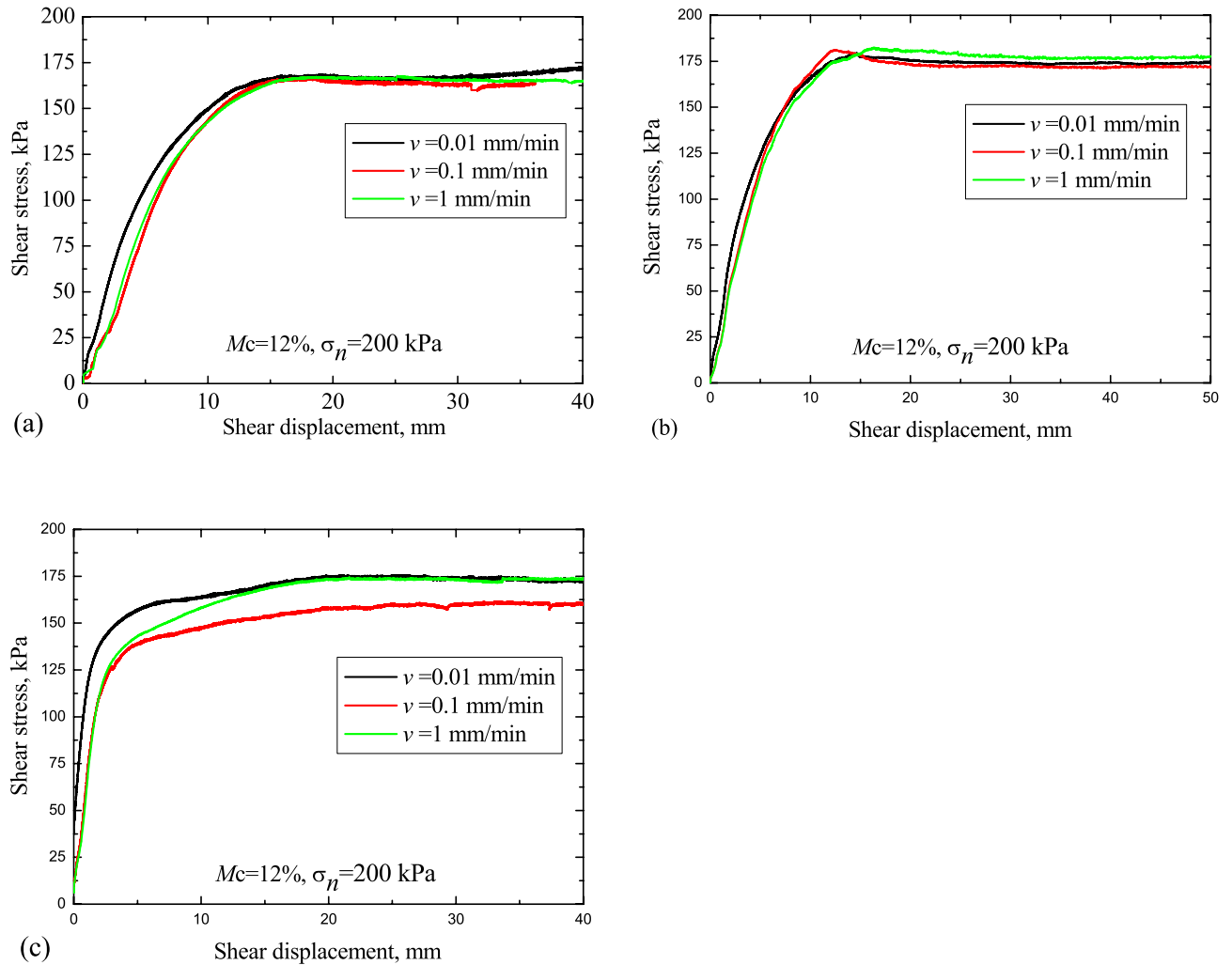


Figure 8. Shear stress versus shear displacement. (a) Loess; (b) red clay; (c) LRCl.

By fitting the experimental data in Fig. 9a, the relationships between the peak shear strength and the moisture content for loess, red clay and LRCl were expressed as follows, respectively:

$$\tau_p = 237.36e^{(-Mc/5.44)} + 141.51, \quad 12 \leq Mc \leq 28 \tag{1}$$

$$\tau_p = 609.55e^{(-Mc/5.71)} + 108.25, \quad 12 \leq Mc \leq 28 \tag{2}$$

$$\tau_p = 223.33e^{(-Mc/9.89)} + 108.13, \quad 12 \leq Mc \leq 28 \tag{3}$$

In addition, the variation in the residual shear strength with moisture content of loess, red clay and LRCl were written as follows by fitting the experimental data in Fig. 9b:

$$\tau_r = 216.78e^{(-Mc/5.70)} + 138.99, \quad 12 \leq Mc \leq 28 \tag{4}$$

$$\tau_r = 255.19e^{(-Mc/8.93)} + 106.91, \quad 12 \leq Mc \leq 28 \tag{5}$$

$$\tau_r = 538.32e^{(-Mc/6.34)} + 99.36, \quad 12 \leq Mc \leq 28 \tag{6}$$

It can be seen from Eqs. (1–6) that: both the peak strength and the residual strength decreased with the increase of moisture content for all specimens, consistent with the observations from tests reported in other studies^{13,31}. Meanwhile, it has been shown that the shear resistance of red clay samples is more sensitive to the variation of moisture content compared with that of loess and LRCl samples. The correlations between the shear strength and moisture content were obtained and shown in Eqs. (1)–(6), which can be used to quantitatively understand the triggering mechanism of such kind of landslides and to predict the landslides evolution in future by combining with numerical simulation methods.

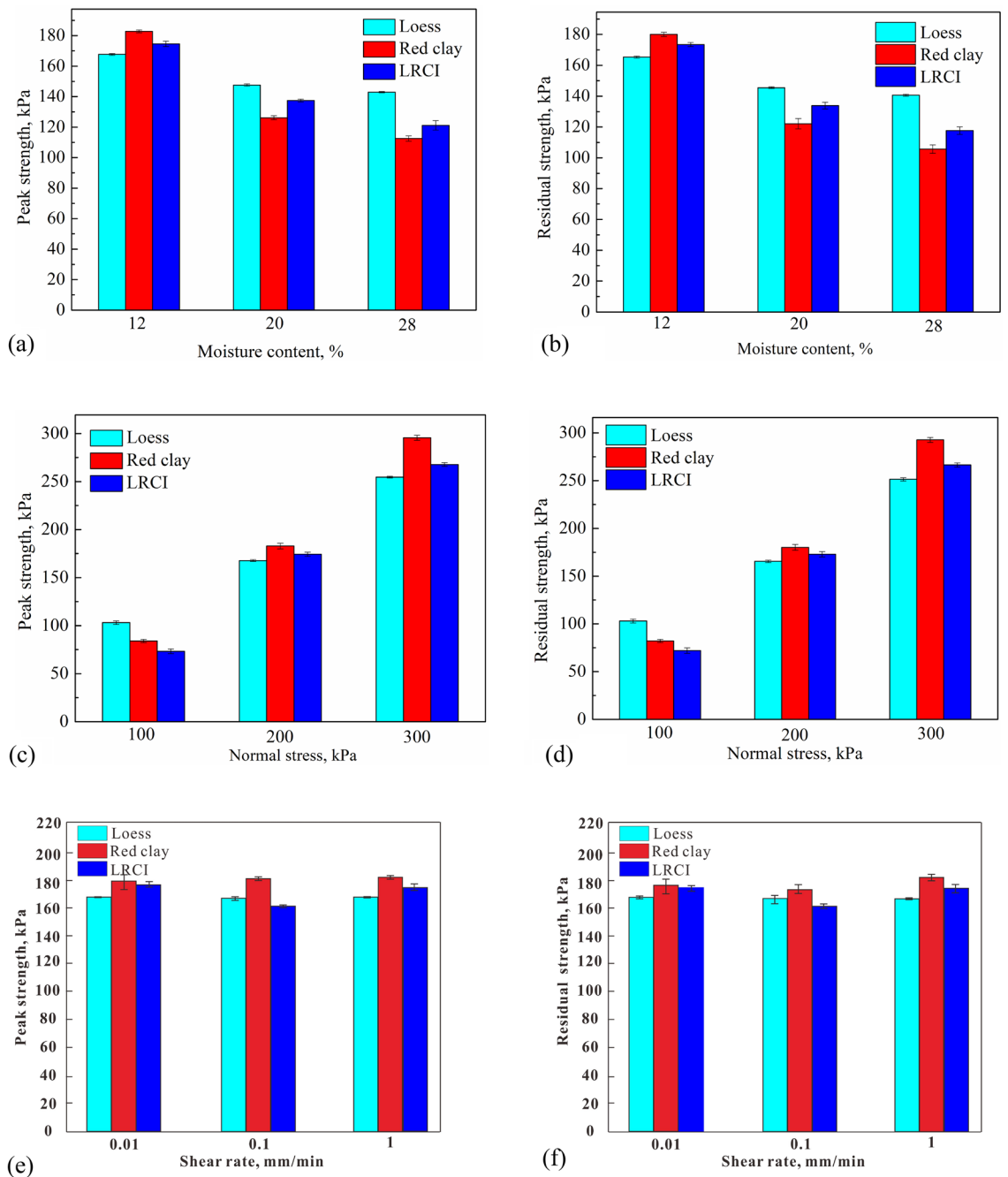


Figure 9. Histograms depicting peak strength and residual strength. (a,b) with moisture content; (c,d) with normal stress; (e,f) with shear rate. Error bars represent standard error (n = 3).

The relationship between shear stress and shear displacement under different normal stresses is shown in Fig. 7. It can be found that: (1) as normal stress increases, both the peak shear strength and the residual shear strength shows an increasing tendency; (2) LRCI specimen is greatest affected by the normal stress, followed by red clay, and the loess specimen is least affected by the normal stress. To be more specific, the magnitude of τ_r of LRCI specimen at normal stress of 300 kPa (266.47 kPa) is 3.7 times the magnitude of τ_r at normal stress of 100 kPa (72.03 kPa). As for red clay specimen, the τ_r at normal stress of 300 kPa (292.76 kPa) equals to 3.56 times the τ_r at normal stress of 100 kPa (82.15 kPa). Comparatively, an increase from 100 to 300 kPa of normal stress of loess specimen result in an increase of the τ_r from around 103.01 kPa to 251.39 kPa, i.e., more than 2.4 times (Fig. 9d). This study shows that residual strength increases with normal stress, a finding that agrees with a number of previous studies^{41,42}.

By now, it has been found that the residual shear strength of soil may be positively dependent, negatively dependent on shear rates or unrelated with shear rates^{32,33,43–45}. The experimental results shown in Fig. 9e,f revealed that the effect of shear rate on the shear strength is almost negligible, which is consistent with the

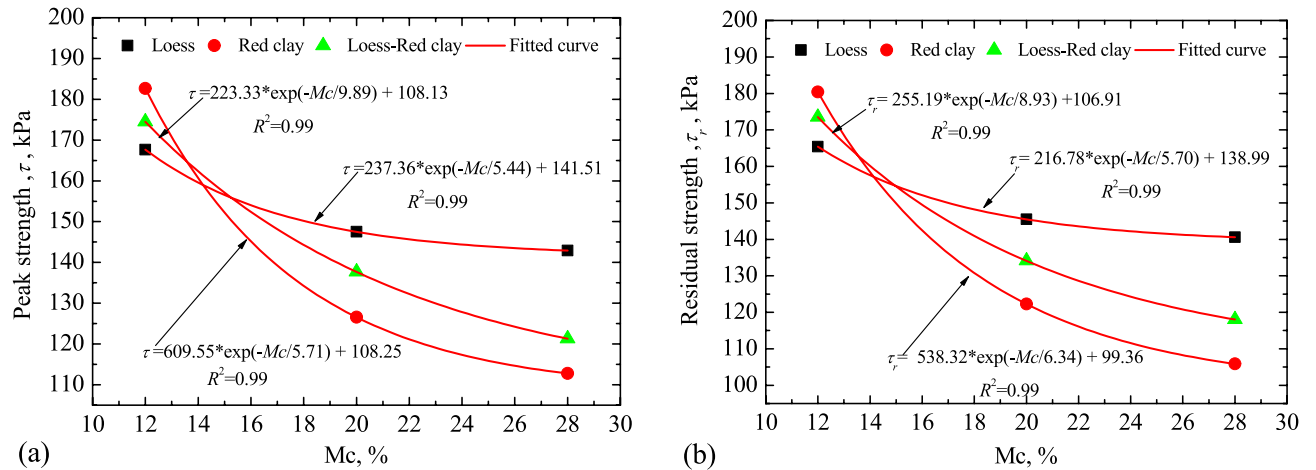


Figure 10. Relationship between shear strength and moisture content. (a) Peak shear strength; (b) residual shear strength.

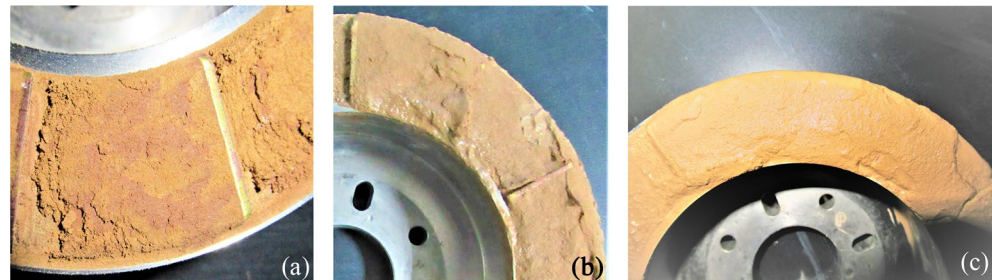


Figure 11. Macroscopic morphology of LRCI Shear Surface with different moisture contents ($\sigma_n = 200$ kPa, $v = 1$ mm/min). (a) Mc = 12%; (b) Mc = 20%; (c) Mc = 28%.

previous studies^{33,45,46}, in which they reported that shear rate has little effect on the shear strength with shear rate lower than 10 mm/min.

Macroscopic observation in the morphology of LRCI shear surface. The macroscopic morphology of LRCI shear surface at different moisture contents is shown in Fig. 11. A localized water accumulation was developed within the shear plane at the moisture content of 20% (Fig. 11b). Meanwhile, a high degree of liquefaction phenomenon was clearly observed at the moisture content of about 28% (close to the saturation degree) in Fig. 11c. Other studies^{10,33,47} similarly reported the occurrences of the liquefaction in shear plane of saturated loess samples. Such phenomenon can be explained as follows: during the shearing process, a smooth shear plane develops within the LRCI specimen (Fig. 11a), which is consistent with the conclusion reported by some researchers^{37,48} that a smooth shear plane appears in the clay-rich soil when the shear displacement is large enough^{29,35}. As moisture content increases, the soil matrix suction decreases gradually⁴⁹, and eventually more free water accumulates on the shear plane, causing liquefaction of the soil sample, which also lubricates the soil particles near shear plane and thus reduces the frictional bite force between the soil particles. Therefore, the shear strength of the sample gradually decreases as water content increases (Fig. 9a,b). It has been acknowledged that the occurrence of a loess landslide is usually attributed to static liquefaction^{50,51}. The experimental results indicated that the LRCI soils with a relatively high degree of saturation shows the potential of localized liquefaction which may be related to the occurrence of a loess-red clay landslide with high-speed and long-run out. The particle size distribution of LRCI shear surface, determined using a Mastersizer 2000 (UK) laser particle size analyzer, shows that compared with specimen prior to shearing, the fine particle content increased after shearing (Fig. 12).

Change in the microstructure of the shear surface with moisture content. It should be noted that the significance of microstructure in evaluation of the deformation and shear strength characteristics of soil^{38,52}. Furthermore, the change in the microstructure of slip zone soils during the shearing process is complicated⁵³ and the macroscopic mechanical properties of soils could be directly related to its microstructure^{54,55}. Therefore, to exemplify the variation in the microstructure of samples, scanning electron microscopy (SEM) tests were conducted on shear planes of specimens at different moisture contents levels. After the ring shear tests, air-drying

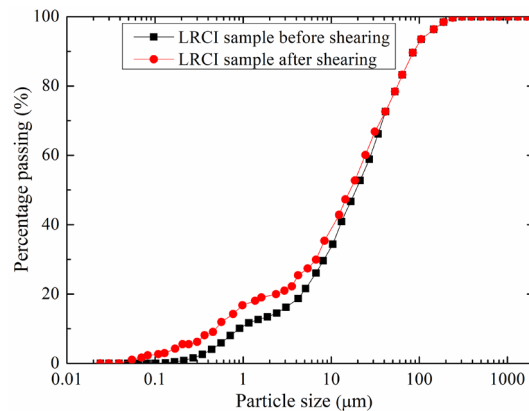


Figure 12. Particle size distribution of LRCI shear surface before and after shearing.

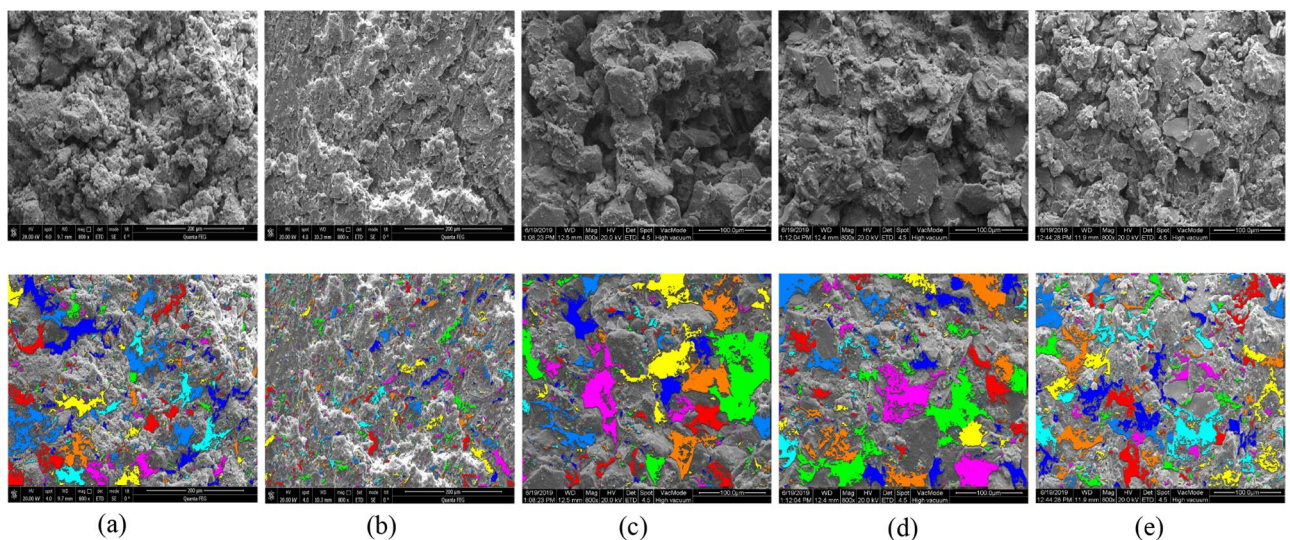


Figure 13. SEM images of shear surface with different moisture contents ($800\times$, $\sigma_n=200$ kPa, $v=1$ mm/min). (a) Loess, $Mc=12\%$; (b) red clay, $Mc=12\%$; (c) LRCI, $Mc=12\%$; (d) LRCI, $Mc=20\%$; (e) LRCI, $Mc=28\%$.

shear planes with area of about 1 mm^2 were used to conduct SEM tests. The SEM images of loess, red clay and LRCI samples are shown in Fig. 13a–e.

From Fig. 13a–e, it can be seen that the microstructure characteristics of shear surfaces obtained from three kinds of specimens with the moisture content of 12% are as follows: the structure of loess is mainly composed of macro-pores with various sizes (Fig. 13a). For the red clay dominated by mineral components such as montmorillonite and illite^{7,10}, the flake microstructure appears within shear surface (Fig. 13b), which may be attributed to the rearrangement of flaky particles with obvious reorientation¹³. Nevertheless, LRCI is a mixture of loess and red clay granules, within which the contact between the flaky particles is not very tight due to the existence of pores (Fig. 13c) and flaky particles show some degree of preferred orientation. From a microscopic viewpoint, the LRCI sample (Fig. 13c) has more porosity than the red clay sample (Fig. 13b). Consequently, the attraction between the soil particles of LRCI sample becomes smaller, resulting in a reduction in shear strength (Figs. 9, 10).

With an increase in moisture content of LRCI specimen, the shear surface becomes smoother and the larger percentage of small-sized pores are observed (Fig. 13c–e). In addition, from the perspective of mineral composition, the flaky clay mineral particles in the LRCI sample are characterized by a strong adsorption capacity. Thus, the hydrated film is thickened and expanded⁵⁶ when more water infiltrates into the LRCI sample. Consequently, the sliding friction is vulnerable to occurring between the granules, leading to a great reduction in the shear strength with increasing moisture content.

To quantitatively clarify the effect of moisture content on the micro-porosity parameters including surface porosity (P) and Mean Pore Area (\bar{S}_v), Avizo9.0 software was adopted to process Fig. 13a–e following previous studies (Wong et al., 2018; Hu et al., 2018), with which the skeleton algorithm was applied to segment a single pore of the image (Suuronen et al., 2013; Sarkar and Siddiqua 2016) and the results are shown in Figs. 13a'–e'. Surface porosity, denoted by P , is expressed as:

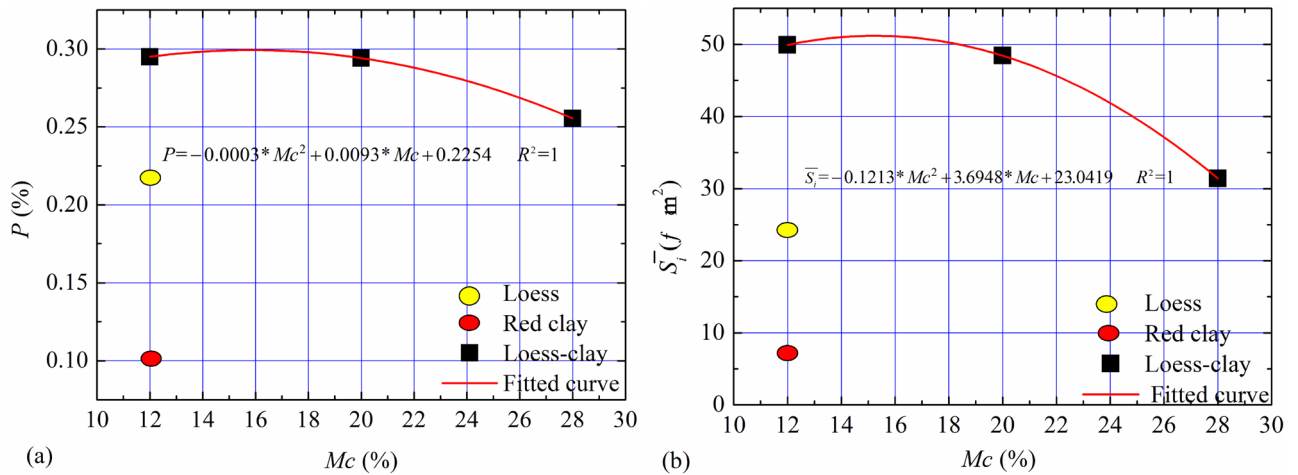


Figure 14. The micro-porosity parameters. (a) Surface porosity, (b) mean pore area.

Sample type	Surface porosity (%)	Mean pore area (μm^2)
Loess (Mc = 12%)	0.217	23.966
Red clay (Mc = 12%)	0.099	7.115
LRCI (Mc = 12%)	0.295	48.919
LRCI (Mc = 20%)	0.294	48.434
LRCI (Mc = 28%)	0.255	31.428

Table 3. The micro-porosity parameters.

$$P = \frac{\Sigma N}{N_{length} \times N_{width}} \tag{7}$$

where N_{length} and N_{width} are the number of pixels of the long and short sides of the image, respectively, and N is the number of pixels of the pore.

Mean Pore Area which is denoted as \bar{S}_i , is given as:

$$\bar{S}_i = \frac{\sum S_i}{N_p}, \quad S_i = N_i \times L_{voxel}^2, \tag{8}$$

where S_i is the area of the i th pore, N_p is the total number of pores, N_i is the number of pixels of the i th pore; L_{voxel} is image resolution.

To quantitatively clarify the effect of moisture content on the micro-porosity parameters of the LRCI specimen, the data in Fig. 14 were fitted as follows:

$$P = -0.0003 * Mc^2 + 0.0093 * Mc + 0.2254 \quad 12 < Mc < 28 \tag{9}$$

$$\bar{S}_i = -0.1213 * Mc^2 + 3.6948 * Mc + 23.0419 \quad 12 < Mc < 28 \tag{10}$$

The estimated surface porosity and mean pore area is listed in Table 3 and plotted in Fig. 14. As shown in Fig. 14, at the same moisture content (Mc = 12%), Surface porosity (P) and Mean Pore Area (\bar{S}_i) of the LRCI sample is greatest while those values of the red clay sample are the minimum (Fig. 14). Additionally, moisture content plays a very significant role in the micro-parameters of LRCI specimen. For example, the surface porosity decreases from 48.919 to 31.42 μm^2 with moisture content ranging from 12 to 28%, and a drop in the mean pore area of nearly 13% (from 0.295% to 0.255%) for LRCI specimen with moisture content ranging from 12 to 28% is observed.

Discussion

Triggering mechanism of loess-red clay landslides. The occurrence of the loess-red clay landslides may be associated with the steep slope, slope structure, physical and mechanical properties of the loess, red clay and the nature of the loess-red clay contact. Based on the geological setting of the slope and the variations of shear resistance of the loess, red clay and LRCI samples, the triggering mechanism of a landslide occurred along a contact between loess soils and red clay can be explained as follows: the steep topography of the slope

with a great gradient (Fig. 1), indicates that the slope is susceptible to instability. In the season with intense precipitation, precipitation easily infiltrates into the loess along the upper cracks when the overlying loess is characterized by a great height difference and free surfaces (Fig. 1). Compared with loess soils, the red clay is poorly permeable¹⁰, which easily causes the water accumulation on the contact between loess and red clay (Fig. 11). Consequently, the contact surface between loess and red clay layer is softened by water infiltration^{6,18}, which causes the mechanical behavior of the contact surface to significantly decrease (Fig. 9) and to develop a softened interlayer (which also be called as weak zone). From a micro perspective, with increase in moisture content due to infiltration into the weak zone, cementing materials such as organic matter and soluble salts in LRCI soils gradually decrease and even disappear, and some clay aggregations are softened or disintegrated⁵⁷. In addition, further increase in the moisture content caused by heavy rainfall would result in the dissolution and leaching of mineral materials such as CaCO₃ (also serving as cementing material) as well⁵⁸. With the disintegration of the cementing materials, the space for soil particle shearing increases. Eventually, the skeleton soil particles within shear zone are rearranged and reoriented and thus a relatively closely particle structure of LRCI is reached (Fig. 13). Furthermore, the disintegrated cementing materials also rearrange due to the adjustment of soil particles. Consequently, some larger pores in LRCI soils are transformed into smaller pores (Figs. 13, 14). Therefore, the initial open structure of LRCI soils becomes a relatively uniform and close structure³⁹ in which the permeability of soils within shear zone decreased dramatically. Accordingly, the pore water moves into the small-sized pores and the built-up excess pore water pressure is difficult to be dissipated due to a close structure of small-sized pores. Owing to the low permeability, high pore-water pressure built up within the shear zone and the increase in the fine particle content (Fig. 12), the LRCI soils with a high saturation degree shows the potential for the localized liquefaction within shear zone (Fig. 11). Once the shear resistance reached up to the shear strength of weak zone surface, the shear surface develops into the sliding surface and the overlying strata in the slopes slides along the sliding surface and eventually leads to the slope failure.

The limitation of experiment and the future work. Firstly, under the effect of gravity of the overlying loess soils, the shear surface of the slip zone soil of the loess-red clay landslide is not actually the circular plane shown in the current study, but a more complicated curved surface. Thus, ring shear tests with more practical curved shear surfaces would be explored with an advanced equipment and technology in future. Secondly, due to the difficulties in the sample preparation, only three sets of ring shear tests with different moisture contents were conducted. Thus, the quantification of correlation given can only describe the relationship between the shear strength and moisture contents in a small range. Therefore, a large number of ring shear tests with moisture contents in a wide range are needed to be done in the future. In addition, the composition of slip zone soil is not the simple materials contacting between loess and red clay in some practical engineering, but a mixture soil of loess and red clay with a certain thickness. Furthermore, the mixing ratio of such mixed soil tends to vary at different locations in the slip zone²³ with influencing factors such as clay content⁴⁰, clay mineral composition⁶⁰, shape and gradation of soil particles¹³, microstructure⁶¹ and stress¹⁶. Therefore, the determination of shear strength of slip zone soils is complicated and challenging^{29,62}. Further experimental studies on slip zone soil of loess-red clay landslides, which focuses on considering limitations of the experiments mentioned above, would be performed in our future research to examine the validity of the above-mentioned test results in the movement prediction of loess-red clay landslides.

Conclusions

Basing on the results of ring shear tests on the loess soils, red clay soils taken from a typical loess-red clay landslide in Loess Plateau Hinterland and LRCI specimens, the mechanical properties of slip zones between loess and red clays as well as the triggering mechanism of loess-red clay landslides were discussed. The following conclusions were drawn:

- (i) Both the peak and residual strength of loess, red clay and LRCI specimen decrease exponentially with increasing moisture content. Among which, the moisture content has the greatest influence on the peak and residual strength of red clay, followed by the LRCI specimen, and the loess specimen is least affected. In addition, with the moisture content above a certain value, shear resistance of LRCI and red clay is dramatically less than that of the loess specimen.
- (ii) Ring shear tests on loess soils, red clay and LRCI specimens showed that the peak and residual strength of soils is dependent upon normal stress. There is a positive correlation between the normal stress and increase in shear resistance. In addition, LRCI specimen is greatest affected by normal stress, followed by red clay, and the loess specimen is least influenced by the normal stress.
- (iii) The macroscopic morphological characteristics of shear surface obtained from the LRCI specimens demonstrated that a localized water accumulation was built up within the shear surface as the water content increases to some extent, and a high degree of liquefaction developed within specimen when the moisture content reaches to the saturated degree., which shows the potential of localized liquefaction which may be related to the occurrence of a loess-red clay landslide.
- (iv) The microstructural testing results show that with an increase in moisture content of LRCI specimen, the shear surface become smoother and the larger percentage of small-sized pores are observed. Accordingly, the pore water moves into the small-sized pores and the built-up excess pore water pressure is difficult to be dissipated due to a close structure of small-sized pores. Owing to the low permeability, high pore-water pressure built up within the shear zone and the increase in the fine particle content, the LRCI soils with a high saturation degree shows the potential for the localized liquefaction within shear zone, which

further provides a scientific explanation for the occurrence of loess-red clay landslides with high-speed and long run out.

Received: 10 January 2021; Accepted: 3 August 2021

Published online: 02 September 2021

References

- Dijkstra, T. *et al.* The loess of north-central China: Geotechnical properties and their relation to slope stability. *Eng. Geol.* **36**(3–4), 153–171 (1994).
- Meng, X., Derbyshire, E. & Kemp, R. A. Origin of the magnetic susceptibility signal in Chinese loess. *Quatern. Sci. Rev.* **16**(8), 833–839 (1997).
- Derbyshire, E. Geological hazards in loess terrain, with particular reference to the loess regions of China. *Earth Sci. Rev.* **54**(1–3), 231–260 (2001).
- Qiu, H. *et al.* Influence of topography and volume on mobility of loess slides within different slip surfaces. *CATENA* **157**, 180–188 (2017).
- Peng, J. *et al.* Landslides triggered by excavation in the loess plateau of China: A case study of Middle Pleistocene loess slopes. *J. Asian Earth Sci.* **171**, 246–258 (2019).
- Zhang, M. & Liu, J. Controlling factors of loess landslides in western China. *Environ. Earth Sci.* **59**(8), 1671–1680 (2010).
- Shi, J. *et al.* Neogene clay and its relation to landslides in the southwestern Loess Plateau, China. *Environ. Earth Sci.* **77**(5), 204 (2018).
- Chen, J. *et al.* Properties and microstructure of a natural slip zone in loose deposits of red beds, southwestern China. *Eng. Geol.* **183**, 53–64 (2014).
- Wen, B. P. & Aydin, A. Microstructural study of a natural slip zone: Quantification and deformation history. *Eng. Geol.* **68**(3), 289–317 (2003).
- Zhang, Z. *et al.* Dynamics characteristic of red clay in a deep-seated landslide, Northwest China: An experiment study. *Eng. Geol.* **239**, 254–268 (2018).
- Shi, J. *et al.* Analysis of the causes of large-scale loess landslides in Baoji, China. *Geomorphology* **264**, 109–117 (2016).
- Li, B., Wu, S. & Shi, J. Engineering geological properties and hazard effects of Hipparion laterite in Baoji, Shaanxi Province. *Geol. Bull. China* **32**(12), 1918–1924 (2013).
- Wen, B.-P. & He, L. Influence of lixiviation by irrigation water on residual shear strength of weathered red mudstone in Northwest China: Implication for its role in landslides' reactivation. *Eng. Geol.* **151**, 56–63 (2012).
- Qiu, H. *et al.* Slope height and slope gradient controls on the loess slide size within different slip surfaces. *Phys. Geogr.* **38**(4), 303–317 (2017).
- Junhong, H., Zhenguo, Z. & Weiqiang, C. The change of natural zones and the evolution of red earth in china. *Acta Geogr. Sinica* **54**(3), 193–203 (1999).
- Wang, Q. *et al.* Geological and geotechnical characteristics of laterite in northwestern China. *Quat. Int.* **519**, 263–273 (2019).
- Xu, L. *et al.* Landslides in a loess platform, North-West China. *Landslides* **11**(6), 993–1005 (2014).
- Li, B., Feng, Z. & Wang, W. Characteristics of the Sanmen Formation clays and their relationship with loess landslides in the Guanzhong area, Shaanxi, China. *Arab. J. Geosci.* **8**(10), 7831–7843 (2015).
- Lian, B. *et al.* Moisture content effect on the ring shear characteristics of slip zone loess at high shearing rates. *Bull. Eng. Geol. Environ.* **79**(2), 999–1008 (2020).
- Wang, H. *et al.* Characteristic analysis of large-scale loess landslides: a case study in Baoji City of Loess Plateau of Northwest China. *Nat. Hazard.* **11**(7), 1829–1837 (2011).
- Zhang, F. *et al.* Undrained shear behavior of loess saturated with different concentrations of sodium chloride solution. *Eng. Geol.* **155**, 69–79 (2013).
- Hou, K. *et al.* Influence of Quaternary paleoclimate change on the permeability of the loess–paleosol sequence in the Loess Plateau, northern China. *Earth Surf. Proc. Land.* **45**(4), 862–876 (2020).
- Wen, B. *et al.* Deformation Characteristics of Loess Landslide along the Contact between Loess and Neocene Red Mudstone. *Acta Geol. Sinica – Engl. Ed.* **79**(1), 139–151 (2005).
- Duan, W. *et al.* In-situ evaluation of undrained shear strength from seismic piezocone penetration tests for soft marine clay in Jiangsu, China. *Transp. Geotech.* **20**, 100253 (2019).
- Duan, W., *et al.* A hybrid GMDH neural network and logistic regression framework for state parameter-based liquefaction evaluation. *Can. Geotech. J.* (2021).
- Hu, S. *et al.* Acquiring high-resolution topography and performing spatial analysis of loess landslides by using low-cost UAVs. *Landslides* **15**(3), 593–612 (2018).
- Di Maio, C., Vassallo, R. & Vallario, M. Plastic and viscous shear displacements of a deep and very slow landslide in stiff clay formation. *Eng. Geol.* **162**, 53–66 (2013).
- Di Maio, C., Scaringi, G. & Vassallo, R. Residual strength and creep behaviour on the slip surface of specimens of a landslide in marine origin clay shales: influence of pore fluid composition. *Landslides* **12**(4), 657–667 (2015).
- Skempton, A. W. Long-term stability of clay slopes. *Geotechnique* **14**(2), 77–102 (1964).
- Sun, P. *et al.* Physical model experiments for shallow failure in rainfall-triggered loess slope, Northwest China. *Bull. Eng. Geol. Environ.* **78**(6), 4363–4382 (2019).
- Jiang, Y. *et al.* Influence of initial dry density and water content on the soil–water characteristic curve and suction stress of a reconstituted loess soil. *Bull. Eng. Geol. Environ.* **76**(3), 1085–1095 (2017).
- Wang, G., Suemine, A. & Schulz, W. H. Shear-rate-dependent strength control on the dynamics of rainfall-triggered landslides, Tokushima Prefecture, Japan. *Earth Surf. Processes Landf.* **35**(4), 407–416 (2010).
- Wang, G. *et al.* Pore-pressure generation and fluidization in a loess landslide triggered by the 1920 Haiyuan earthquake, China: A case study. *Eng. Geol.* **174**, 36–45 (2014).
- Prodan, M. V. *et al.* Influence of weathering processes on the shear strength of siltstones from a flysch rock mass along the northern Adriatic coast of Croatia. *Bull. Eng. Geol. Environ.* **76**(2), 695–711 (2017).
- Vithana, S. B. *et al.* Correlation of large displacement drained shear strength of landslide soils measured by direct shear and ring shear devices. *Landslides* **9**(3), 305–314 (2012).
- Sassa, K. *et al.* Undrained dynamic-loading ring-shear apparatus and its application to landslide dynamics. *Landslides* **1**(1), 7–19 (2004).
- Bishop, A. W. *et al.* A new ring shear apparatus and its application to the measurement of residual strength. *Geotechnique* **21**(4), 273–328 (1971).
- Salih, W. T. *et al.* Study on stress–strain–resistivity and microscopic mechanism of red mud waste modified by desulphurization gypsum-fly ash under drying–wetting cycles. *Constr. Build. Mater.* **249**, 118772 (2020).

39. Lian, B. *et al.* Mechanical response of root-reinforced loess with various water contents. *Soil Tillage Res.* **193**, 85–94 (2019).
40. Derbyshire, E. *et al.* Failure mechanisms in loess and the effects of moisture content changes on remoulded strength. *Quatern. Int.* **24**, 5–15 (1994).
41. Chen, X. & Liu, D. Residual strength of slip zone soils. *Landslides* **11**(2), 305–314 (2014).
42. Vithana, S. B. *et al.* Effects of overconsolidation ratios on the shear strength of remoulded slip surface soils in ring shear. *Eng. Geol.* **131**, 29–36 (2012).
43. Gratchev, I. B. & Sassa, K. Shear strength of clay at different shear rates. *J. Geotech. Geoenviron. Eng.* **141**(5), 06015002 (2015).
44. Kimura, S. *et al.* Shearing rate effect on residual strength of landslide soils in the slow rate range. *Landslides* **11**(6), 969–979 (2014).
45. Scaringi, G. & Di Maio, C. Influence of displacement rate on residual shear strength of clays. *Procedia Earth Planet. Sci.* **16**, 137–145 (2016).
46. Skempton, A. W. Residual strength of clays in landslides, folded strata and the laboratory. *Geotechnique* **35**(1), 3–18 (1985).
47. Zhang, D. & Wang, G. Study of the 1920 Haiyuan earthquake-induced landslides in loess (China). *Eng. Geol.* **94**(1–2), 76–88 (2007).
48. Nakamura, S. *et al.* Platy layer silicate minerals for controlling residual strength in landslide soils of different origins and geology. *Geology* **38**(8), 743–746 (2010).
49. Lu, N. & Likos, W. J. Suction stress characteristic curve for unsaturated soil. *J. Geotech. Geoenviron. Eng.* **132**(2), 131–142 (2006).
50. Zhou, Y. F. *et al.* Laboratory study on soil behavior in loess slope subjected to infiltration. *Eng. Geol.* **183**, 31–38 (2014).
51. Qi, X., Xu, Q. & Liu, F. Analysis of retrogressive loess flowslides in Heifangtai, China. *Eng. Geol.* **236**, 119–128 (2018).
52. Terzaghi, K., Mesri, G. & Peck R. B. *Soil Mechanics in Engineering Practice* 3rd edn (1996).
53. Tchalenko, J. & Morgenstern, N. Microscopic Structures in Kaolin Subjected to Direct Shear. *Géotechnique*, **17**(4), 309–328 (1967).
54. Osipov, B. *The Natural Features on Strength and Deformation of Clayey Soil and Rocks* 1–60 (Press House of Geology, 1985).
55. Jiang, M. *et al.* Structural characterization of natural loess and remolded loess under triaxial tests. *Eng. Geol.* **181**, 249–260 (2014).
56. Nguana, W. B. F. & Kalinichev, A. G. Structural arrangements of isomorphic substitutions in smectites: Molecular simulation of the swelling properties, interlayer structure, and dynamics of hydrated Cs–montmorillonite revisited with new clay models. *J. Phys. Chem. C* **118**(24), 12758–12773 (2014).
57. Li, P. *et al.* Microstructural evolution of loess soils from the Loess Plateau of China. *CATENA* **173**, 276–288 (2019).
58. Zhao, J. *et al.* Soil characteristics and new formation model of loess on the Chinese Loess Plateau. *Geosci. J.* **21**(4), 607–616 (2017).
59. Li, X.-A. *et al.* Characterization of the mechanisms underlying loess collapsibility for land-creation project in Shaanxi Province, China—A study from a micro perspective. *Eng. Geol.* **249**, 77–88 (2019).
60. Skinner, A. E. A note on the influence of interparticle friction on the shearing strength of a random assembly of spherical particles. *Géotechnique* **19**(1), 150–157 (1969).
61. Xu, L. & Coop, M. R. Influence of structure on the behavior of a saturated clayey loess. *Can. Geotech. J.* **53**(6), 1026–1037 (2016).
62. Olson, R. E. Shearing strengths of kaolinite, illite, and montmorillonite. *J. Geotech. Geoenviron. Eng.* **102**(GT2), 180–182 (1976).

Acknowledgements

This research was supported by the National Natural Science Foundation of China (No.41902268) and the China Postdoctoral Science Foundation (No. 2019T120871).

Author contributions

B.L. and X.W. proposed the method, performed the analysis and primarily wrote the article. K.L. participated in composing the paper. S.H. and X.F. provided the data for the case studies. Each of the authors reviewed the manuscript prior to submission. The authors declare that they have no known competing financial interests or personal relationships that could have appeared to influence the work reported in this paper.

Competing interests

The authors declare no competing interests.

Additional information

Correspondence and requests for materials should be addressed to X.W.

Reprints and permissions information is available at www.nature.com/reprints.

Publisher's note Springer Nature remains neutral with regard to jurisdictional claims in published maps and institutional affiliations.



Open Access This article is licensed under a Creative Commons Attribution 4.0 International License, which permits use, sharing, adaptation, distribution and reproduction in any medium or format, as long as you give appropriate credit to the original author(s) and the source, provide a link to the Creative Commons licence, and indicate if changes were made. The images or other third party material in this article are included in the article's Creative Commons licence, unless indicated otherwise in a credit line to the material. If material is not included in the article's Creative Commons licence and your intended use is not permitted by statutory regulation or exceeds the permitted use, you will need to obtain permission directly from the copyright holder. To view a copy of this licence, visit <http://creativecommons.org/licenses/by/4.0/>.

© The Author(s) 2021